Mechanics Research Communications 148 (2025) 104479

Contents lists available at ScienceDirect

Mechanics Research Communications

journal homepage: www.elsevier.com/locate/mechrescom

Finite difference displacement integration for linear buckling analysis of non-uniform columns

Paolo Di Re

Department of Structural and Geotechnical Engineering, Sapienza University of Rome, Via Eudossiana 18, 00184 Rome, Italy

ARTICLE INFO

Keywords:
Beam
Geometric nonlinearity
Buckling
Force-based model
Finite difference method

ABSTRACT

This paper proposes the use of the Finite Difference Displacement Integration (FDDI) technique for the numerical analysis of columns subjected to flexural buckling. The proposed method for buckling analysis is based on the approach suggested by other researchers, who have used the Curvature Based Displacement Interpolation (CBDI) technique. The CBDI technique, formulated within the realm of geometrically nonlinear force-based frame elements, employs a Lagrange interpolation of the cross-section bending curvature. However, this has shown numerical instability when numerous quadrature cross-sections are placed along the element length. Consequently, the proposed buckling analysis method is revisited with the incorporation of the FDDI technique, which employs a finite difference approximation of the cross-section compatibility conditions, yielding a more robust, yet computationally equivalent numerical method. Numerical tests are conducted to evaluate the efficacy of the proposed method, demonstrating that the FDDI effectively eliminates numerical difficulties and reliably converges to the exact solution.

1. Introduction

Flexural buckling is an essential phenomenon to consider in the design and safety assessment of vertical structural components, including bridge piers and slender columns, as it can markedly decrease the load bearing capacity of the structure. However, flexural buckling depends on the flexural stiffness, which may vary throughout the height of the element due to nonprismatic geometries or material alterations such as plasticity, damage, corrosion, or other factors. In these cases, determining the buckling response is complicated and requires advanced mathematical procedures. Analytical approaches frequently include solving differential equations that characterize the column behavior with variable stiffness functions [1–4]. Since closed-form solutions are not always available, simplified [5–8] or numerical approaches [9,10] are frequently employed. These require the use of sophisticated numerical methods and advanced software, like finite element buckling analysis.

Scott and Denavit [11] proposed a method for calculating the buckling loads of simple columns with arbitrarily variable flexural stiffness. They exploited the Curvature Based Displacement Interpolation (CBDI) method for geometrically nonlinear force-based frame elements and defined a linear buckling eigenvalue problem starting from the definition of the derivative of the column transverse displacements with respect to the element axial force. The method directly accounts for possible stiffness variation along the axis, as the eigenvalue problem relies on the definition of the compatibility matrix between the element transverse displacements and cross-section bending curvatures, as well as the flexibility matrix that describes the stiffness variation of the column.

The CBDI was originally introduced in [12] to compute the transverse displacements in two-dimensional (2D) Euler–Bernoulli beams, by Lagrange interpolation and double integration of the bending curvatures along the element axis. De Souza [13] expanded the technique to three-dimensional (3D) elements, while Jafari et al. [14] and Rezaiee-Pajand and Gharaei-Moghaddam [15] covered the case of Timoshenko elements, by combining the interpolation and integration of the bending curvatures with that of the shear strains (Curvature and Shear Based Displacement Interpolation — CSBDI).

More recently, the CBDI (or CSBDI) technique has been used successfully for enhanced applications by various authors [16–18]. However, some works, e.g. [19], mention that this approach might pose numerical issues, due to oscillatory behavior of the Lagrange interpolation. The work in [11] also shows that, when the CBDI is used for buckling analysis, with a high number of quadrature cross-sections along the element, the method is numerically unstable and fails to converge to the correct solution. Di Re and Benaim Sanchez [20] corroborated these observations, revealing that, when many quadrature cross-sections are considered along the element, numerical errors

E-mail address: paolo.dire@uniroma1.it.

https://doi.org/10.1016/j.mechrescom.2025.104479
Received 20 September 2024; Received in revised form 18 April 2025; Accepted 4 July 2025
Available online 16 July 2025

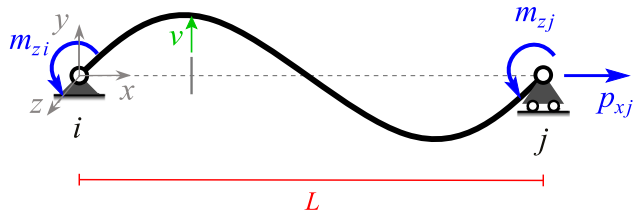

Fig. 1. Element local reference system: element basic nodal forces and cross-section transverse displacement.

arise due to the ill-conditioning of the governing compatibility matrix. As a result, while preserving the same formal architecture of the key governing equations, they devised an alternative technique, for geometrically nonlinear force-based frame elements, that avoids these problems, namely the Finite Difference Displacement Integration (FDDI). This new technique makes use of a finite difference (FD) approximation of the transverse displacement second order derivative, which is equal to the bending curvature, for Euler–Bernoulli beams. However, in [20], the FDDI is applied only to the general model of a force-based frame element under geometrically nonlinear behavior, and application to buckling analysis is not explored.

This work discusses the adoption of the FDDI for the flexural buckling analysis of columns with arbitrarily variable stiffness. The method proposed by [11] is reexamined by replacing the derivations based on the CBDI technique with the alternative definitions obtained from the FDDI, to solve the problems related to the ill-conditioning of the curvature interpolation matrices. After reviewing the force-based beam equilibrium equations, from which the CBDI and FDDI techniques are derived, the definition of the eigenvalue problem for buckling analysis of a general column is described in a unified formulation that alternatively permits the adoption of either the CBDI or the FDDI. Hence, two numerical tests are performed to study the effectiveness of the proposed strategy.

2. Beam equilibrium and transverse displacement computation

Referring to the Euler–Bernoulli beam theory, where shear deformations are neglected, a 2D beam model is considered. This has a straight element axis x, connecting the end nodes i and j, and transverse cross-sections parallel to the orthogonal y-z plane.

If a simply-supported configuration is considered, as in Fig. 1, the basic element forces $\mathbf{q} = \{p_{xj} \quad m_{zi} \quad m_{zj}\}^T$ acting at the nodes are the axial force p_{xj} at node j, and the bending couples m_{zi} and m_{zj} at nodes i and j, respectively. These must be in equilibrium with the beam internal forces (stress resultants) $\mathbf{s}(x) = \{N(x) \quad M_z(x)\}^T$, i.e. the cross-section normal force $N(x)$ and the bending moment $M_z(x)$, which are work-conjugate to the cross-section generalized strains $\mathbf{e}(x)$, i.e. the elongation $\varepsilon_G(x)$ and bending curvature $\chi_z(x)$, respectively.

The equilibrium conditions between $\mathbf{s}(x)$ and $\mathbf{q}$ are expressed in the element deformed configuration, based on the second-order geometry assumption, i.e. the nonlinear coupling between the axial and shear internal forces is neglected [12,13]. Therefore, the following matrix expression results:

$$\underbrace{\begin{Bmatrix} N(x) \\ M_z(x) \end{Bmatrix}}_{\mathbf{s}(x)} = \underbrace{\begin{bmatrix} 1 & 0 & 0 \\ v(x) & \frac{x}{L}-1 & \frac{x}{L} \end{bmatrix}}_{\mathbf{b}(x)} \underbrace{\begin{Bmatrix} p_{xj} \\ m_{zi} \\ m_{zj} \end{Bmatrix}}_{\mathbf{q}} \tag{1}$$

where $\mathbf{b}(x)$ is the equilibrium matrix that depends on the cross-section transverse displacements $v(x)$ (Fig. 1), while L is the undeformed element length.

To determine the displacement field $v(x)$, two alternative numerical techniques are employed, namely the Curvature Based Displacement Interpolation (CBDI) [12,13] and the recently proposed Finite Difference Displacement Integration (FDDI) [20]. These give the displacement values at n monitored cross-sections, x_1, x_2, …, x_n, along the beam axis, where the bending curvature $\chi_z(x)$ is assumed to be known. In general, these cross-sections coincide with the quadrature points adopted to numerically perform the integration of the nodal force vector and flexibility matrix. The monitored cross-section displacements and curvatures are collected in the following vectors:

$$\mathbf{V} = \{v(x_1) \quad v(x_2) \quad \dots \quad v(x_n)\}^T \tag{2}$$

$$\mathbf{X}_z = \{\chi_z(x_1) \quad \chi_z(x_2) \quad \dots \quad \chi_z(x_n)\}^T \tag{3}$$

and the relationship between $\mathbf{V}$ and $\mathbf{X}_z$ is as follows:

$$\mathbf{V} = \mathbf{H}_\chi \mathbf{X}_z \tag{4}$$

where $\mathbf{H}_\chi$ is a $n \times n$ matrix, differently defined depending on whether the CBDI or FDDI technique is applied.

2.1. CBDI technique

In the CBDI, the curvatures $\chi_z(x)$ is interpolated along the element axis through Lagrange polynomials and double integration is performed to obtain the displacements $v(x)$, i.e.:

$$\frac{\mathrm{d}^2 v(x)}{\mathrm{d}x^2} = \chi_z(x) \qquad \rightarrow \qquad v(x) = \iint \chi_z(x)\,\mathrm{d}x + c_1\,x + c_2 \tag{5}$$

being c_1 and c_2 integration constants to be determined by imposing the boundary conditions. It results [12,13,15,18]:

$$v(\xi) = \mathbf{h}_\chi(\xi)\,\mathbf{X}_z \tag{6}$$

where the normalized abscissa $\xi = \frac{x}{L}$ is introduced and $\mathbf{h}_\chi(\xi)$ is a row vector that collects the integrals of the Lagrange polynomials. This vector is defined by introducing the Vandermonde matrix $\mathbf{G}$ of the n monitored (quadrature) cross-sections, i.e.:

$$\mathbf{h}_\chi(\xi) = L^2 \left[\frac{1}{2}\left(\xi^2 - \xi\right) \quad \frac{1}{6}\left(\xi^3 - \xi\right) \quad \dots \quad \frac{1}{n(n+1)}\left(\xi^{n+1} - \xi\right)\right] \mathbf{G}^{-1} \tag{7}$$

with:

$$\mathbf{G} = \begin{bmatrix} 1 & \xi_1 & \dots & \xi_1^{n-1} \\ \vdots & \vdots & \ddots & \vdots \\ 1 & \xi_n & \dots & \xi_n^{n-1} \end{bmatrix} \tag{8}$$

Hence, matrix $\mathbf{H}_\chi$ in Eq. (4) is obtained by evaluating $\mathbf{h}_\chi(\xi)$ at all n abscissas:

$$\mathbf{H}_\chi = \begin{bmatrix} \mathbf{h}_\chi(\xi_1) \\ \vdots \\ \mathbf{h}_\chi(\xi_n) \end{bmatrix} \tag{9}$$

According to [19], the use of a large number of quadrature cross-sections along the beam can cause numerical difficulties for the CBDI approach. Indeed, in this case, an oscillatory Lagrange interpolation of the curvatures can create oscillatory variation in the displacements, resulting in inaccurate solutions. The work by Di Re and Benaim Sanchez [20] confirms this result, showing that numerical errors also appear due to the ill-conditioning of matrix $\mathbf{G}$, thus resulting nearly singular and difficult to invert. The same work also proves that, in some simulations, the problem can be alleviated if the inverse of the matrix $\mathbf{G}$ is computed using the Moore–Penrose pseudoinverse [21], or by employing advanced methods, such as LU or QR factorizations [22]. Indeed, these methods permit a more precise numerical evaluation of the inverse of matrix $\mathbf{G}$, even when this matrix is ill-conditioned. However, these only mitigate the error, without solving the problem, and, in many applications, do not guarantee the accuracy of the solution. As shown in the numerical tests reported in Section 4, for buckling analysis, the use of the Moore–Penrose pseudoinverse (or equivalently the LU or QR factorizations) does not improve the solution, which strongly deviates from the correct results when the number of quadrature cross-sections increases.

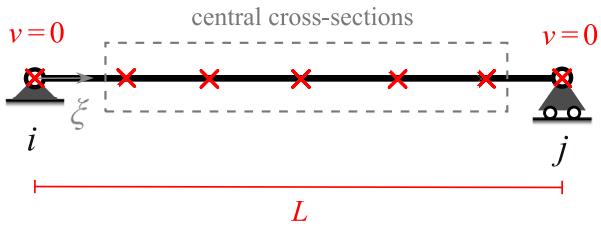

Fig. 2. Partition between the central and the end cross-sections.

2.2. FDDI technique

The FDDI technique relies on the same differential relationship between curvatures $\chi_z(x)$ and transverse displacement $v(x)$ second order derivative as in Eq. (5). However, in this case, the relationship is imposed at all monitored cross-sections and the transverse displacement second order derivative is evaluated by means of FD approximations.

If the two end cross-sections of the element are included in the monitored set (with $n \geq 3$), the simply-supported configuration imposes that $v(0) = v(L) = 0$ (Fig. 2). Therefore, the differential relationship in Eq. (5) can be written for all central cross-sections by expressing the second order derivative of $v(x)$ as a linear combinations of the transverse displacements $\mathbf{V}$ [23–26]. In compact matrix form, it results:

$$\underbrace{\begin{bmatrix} \delta^{(2)}_{22} & \delta^{(2)}_{23} & \cdots & \delta^{(2)}_{2\,n-1} \\ \delta^{(2)}_{32} & \delta^{(2)}_{33} & \cdots & \delta^{(2)}_{3\,n-1} \\ \vdots & \vdots & \ddots & \vdots \\ \delta^{(2)}_{n-1\,2} & \delta^{(2)}_{n-1\,3} & \cdots & \delta^{(2)}_{n-1\,n-1} \end{bmatrix}}_{\boldsymbol{\Delta}^{(2)}_c} \underbrace{\begin{Bmatrix} v(x_2) \\ v(x_3) \\ \vdots \\ v(x_{n-1}) \end{Bmatrix}}_{\mathbf{V}_c} = \underbrace{\begin{Bmatrix} \chi_z(x_2) \\ \chi_z(x_3) \\ \vdots \\ \chi_z(x_{n-1}) \end{Bmatrix}}_{\mathbf{X}_{zc}} \tag{10}$$

where $\mathbf{V}_c$ and $\mathbf{X}_{zc}$ collect the transverse displacements and curvatures, respectively, for the central cross-sections, i.e.:

$$\mathbf{V} = \begin{Bmatrix} v(x_1) & \mathbf{V}_c^T & v(x_n) \end{Bmatrix}^T = \begin{Bmatrix} 0 & \mathbf{V}_c^T & 0 \end{Bmatrix}^T \tag{11}$$

$$\mathbf{X}_z = \begin{Bmatrix} \chi_z(x_1) & \mathbf{X}_{zc}^T & \chi_z(x_n) \end{Bmatrix}^T \tag{12}$$

and $\delta^{(2)}_{\alpha\beta}$, with $\alpha, \beta = 2, \ldots, n-1$, are the FD coefficients that define the second order derivative approximation [20]. These coefficients are computed by means of the *Lagrange interpolation* approach [26], once a specific FD scheme is selected and identified by the scheme order p. In particular, the hth row of matrix $\boldsymbol{\Delta}^{(2)}_c$ contains the FD coefficients associated to the central cross-sections, required to approximate the second order derivative of $v(x)$ at the hth abscissa x_h. Hence, for each row of the matrix, p of the n cross-sections are selected (p-point FD scheme) and the associated coefficients are computed, while the others are set to zero. The general non-zero coefficient $\delta^{(2)}_{hq}$, associated to the qth cross-section, is computed as the second order derivative, evaluated at x_h, of the Lagrange polynomial $\lambda_q(x)$ associated to the qth cross-section, which, in terms of normalized abscissa ξ, results as:

$$\delta^{(2)}_{hq} = \left.\frac{\mathrm{d}^2 \lambda_q(x)}{\mathrm{d}\, x^2}\right|_{x=x_h} = \frac{1}{L^2} \left.\frac{\mathrm{d}^2 \lambda_q(\xi)}{\mathrm{d}\, \xi^2}\right|_{\xi=\xi_h} \tag{13}$$

This computation is simple when the quadrature cross-sections are evenly spaced along the element axis. In fact, in this case, the Lagrange polynomials assume the same expression for all cross-sections, except for the first and last ones, and thus the FD coefficients are almost all equal, requiring little calculation. In the general case of non-uniformly distributed cross-sections, the computation is more demanding. In fact, this requires the definition of all the different Lagrange polynomials and their derivatives, for all different cross-sections, according to Eq. (13). However, Fornberg's recursive algorithm [20,27] exists to perform this computation very efficiently, without defining the Lagrange polynomial

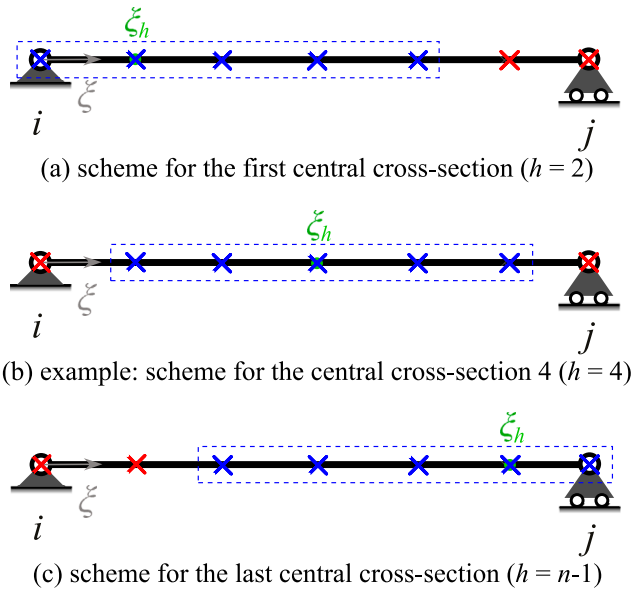

Fig. 3. Cross-section considered for the 5-point FD scheme, highlighting in blue those associated to non-zero coefficients (depicted for $n = 7$). (For interpretation of the references to color in this figure legend, the reader is referred to the web version of this article.)

expressions. To the author knowledge, this algorithm is the best method for computing FD coefficients and is employed in this work.

As an example, Fig. 3 shows the case of the 5-point scheme. This constructs the FD approximation at the hth abscissa over 5 consecutive cross-sections, always including that at $\xi_h = \frac{x_h}{L}$, based on a centered scheme (e.g. Fig. 3b for central cross-section 4), i.e. $[\xi_{h-2}, \xi_{h-1}, \xi_h, \xi_{h+1}, \xi_{h+2}]$. Exception is made for the first and last central cross-sections, for which an asymmetric forward-centered and backward-centered scheme is used, respectively (Figs. 3a and c).

The determination of the coefficients $\delta^{(2)}_{\alpha\beta}$ permits the definition of matrix $\boldsymbol{\Delta}^{(2)}_c$, which is always non-singular [20,26]. Hence, the central cross-section transverse displacements are obtained as follows:

$$\mathbf{V}_c = \left(\boldsymbol{\Delta}^{(2)}_c\right)^{-1} \mathbf{X}_{zc} \tag{14}$$

Finally, by reintroducing the null end values, matrix $\mathbf{H}_\chi$ is obtained, as required in Eq. (4):

$$\mathbf{H}_\chi = \begin{bmatrix} & \mathbf{O}_n & \\ \mathbf{O}_{n-2} & \left(\boldsymbol{\Delta}^{(2)}_c\right)^{-1} & \mathbf{O}_{n-2} \\ & \mathbf{O}_n & \end{bmatrix} \tag{15}$$

being $\mathbf{O}_n$ a null row vector with length n, and $\mathbf{O}_{n-2}$ a null column vector with length $n-2$.

3. Definition of the buckling analysis

Scott and Denavit [11] have shown that, for negligible distributed loads, buckling loads in simple columns, even with variable flexural stiffness, can be determined from the definition of the derivative of the transverse displacement $v(x)$ with respect to the axial force of the beam, that is, $\frac{\mathrm{d}v(x)}{\mathrm{d}p_{xj}}$.

Starting from Eq. (4), this derivative, computed for all cross-sections, results as:

$$\frac{\mathrm{d}\mathbf{V}}{\mathrm{d}p_{xj}} = \mathbf{H}_\chi \frac{\mathrm{d}\mathbf{X}_z}{\mathrm{d}p_{xj}} \tag{16}$$

where the derivatives $\frac{\mathrm{d}\mathbf{X}_z}{\mathrm{d}p_{xj}}$ are obtained as:

$$\frac{\mathrm{d}\mathbf{X}_z}{\mathrm{d}p_{xj}} = \mathrm{diag}\left\{\frac{\mathrm{d}\mathbf{X}_z}{\mathrm{d}N}\right\} \frac{\mathrm{d}\mathbf{N}}{\mathrm{d}p_{xj}} + \mathrm{diag}\left\{\frac{\mathrm{d}\mathbf{X}_z}{\mathrm{d}M_z}\right\} \frac{\mathrm{d}\mathbf{M}_z}{\mathrm{d}p_{xj}} \tag{17}$$

being $\mathbf{N}$ and $\mathbf{M}_z$ column vectors that collect the axial forces and bending moments, respectively, of all cross-sections. From Eq. (1), the derivatives of these internal forces with respect to p_{xj} are equal to:

$$\frac{\mathrm{d}\mathbf{N}}{\mathrm{d}p_{xj}} = \mathbf{1} \quad \text{and} \quad \frac{\mathrm{d}\mathbf{M}_z}{\mathrm{d}p_{xj}} = \mathbf{V} + \frac{\mathrm{d}\mathbf{V}}{\mathrm{d}p_{xj}} p_{xj} \tag{18}$$

where $\mathbf{1}$ is a column vector of length n, with all entries equal to 1. Moreover, the derivatives of the curvatures with respect to the internal forces correspond to the second row of the cross-section flexibility matrix $\mathbf{f}_s(x)$, which governs the constitutive relationship between the internal forces $\mathbf{s}(x)$ and strains $\mathbf{e}(x)$, i.e., in the general incremental form:

$$\underbrace{\begin{Bmatrix} \mathrm{d}\varepsilon_G(x) \\ \mathrm{d}\chi_z(x) \end{Bmatrix}}_{\mathrm{d}\mathbf{e}(x)} = \underbrace{\begin{bmatrix} \frac{\mathrm{d}\varepsilon_G(x)}{\mathrm{d}N} & \frac{\mathrm{d}\varepsilon_G(x)}{\mathrm{d}M_z} \\ \frac{\mathrm{d}\chi_z(x)}{\mathrm{d}N} & \frac{\mathrm{d}\chi_z(x)}{\mathrm{d}M_z} \end{bmatrix}}_{\mathbf{f}_s(x)} \underbrace{\begin{Bmatrix} \mathrm{d}N(x) \\ \mathrm{d}M_z(x) \end{Bmatrix}}_{\mathrm{d}\mathbf{s}(x)} \tag{19}$$

For linear elastic isotropic homogeneous material, the cross-section flexibility results as:

$$\mathbf{f}_s(x) = \begin{bmatrix} EA & -ES_z \\ -ES_z & EI_z \end{bmatrix}^{-1} \tag{20}$$

where E is the material Young's modulus and A, S_z and I_z are the area, the first moment and second moment of area of the cross-section, respectively.

Hence, indicating with $f_{s\,ij}(x_k)$ the term in row i and column j of the flexibility matrix $\mathbf{f}_s(x = x_k)$, it is set:

$$\frac{\mathrm{d}\mathbf{X}_z}{\mathrm{d}N} = \begin{bmatrix} f_{s\,21}(x_1) \\ \vdots \\ f_{s\,21}(x_n) \end{bmatrix} = \mathbf{F}_{s\,21} \quad \text{and} \quad \frac{\mathrm{d}\mathbf{X}_z}{\mathrm{d}M_z} = \begin{bmatrix} f_{s\,22}(x_1) \\ \vdots \\ f_{s\,22}(x_n) \end{bmatrix} = \mathbf{F}_{s\,22} \tag{21}$$

and thus Eq. (17) results as:

$$\frac{\mathrm{d}\mathbf{X}_z}{\mathrm{d}p_{xj}} = \mathrm{diag}\left\{\mathbf{F}_{s\,21}\right\}\mathbf{1} + \mathrm{diag}\left\{\mathbf{F}_{s\,22}\right\}\left(\mathbf{V} + \frac{\mathrm{d}\mathbf{V}}{\mathrm{d}p_{xj}} p_{xj}\right) \tag{22}$$

The expression on the right-hand side of Eq. (22) can be rearranged by introducing matrix $\mathbf{F}_s^*$, which is a block-diagonal matrix that collects all flexibility matrices of all cross-sections, i.e.:

$$\mathbf{F}_s^* = \mathrm{diag}\left\{\mathbf{f}_s(x_1), \mathbf{f}_s(x_2), \ldots, \mathbf{f}_s(x_n)\right\} \tag{23}$$

and matrices $\bar{\mathbf{F}}_s$ and $\bar{\bar{\mathbf{F}}}_s$ defined as [20]:

$$\bar{\mathbf{F}}_s = \mathbf{P}^* \mathbf{F}_s^* \quad \text{and} \quad \bar{\bar{\mathbf{F}}}_s = \mathbf{P}^* \mathbf{F}_s^* \mathbf{P}^{*T} = \mathrm{diag}\left\{\mathbf{F}_{s\,22}\right\} \tag{24}$$

where $\mathbf{P}^*$ is an $n \times 2n$ extraction matrix that, in the first identity of Eq. (24), extracts from $\mathbf{F}_s^*$ all rows related to χ_z, i.e. rows $2, 4, 6, \ldots, 2n$, while, in the second identity, it extracts from $\mathbf{F}_s^*$ the rows related to χ_z and, from these, the columns related to M_z; in other words:

$$\mathbf{P}^* = \begin{bmatrix} 0 & 1 & 0 & 0 & \ldots & 0 & 0 \\ 0 & 0 & 0 & 1 & \ldots & 0 & 0 \\ \vdots & \vdots & \vdots & \vdots & \ddots & \vdots & \vdots \\ 0 & 0 & 0 & 0 & \ldots & 0 & 1 \end{bmatrix} \tag{25}$$

Hence, it results:

$$\frac{\mathrm{d}\mathbf{X}_z}{\mathrm{d}p_{xj}} = \bar{\mathbf{F}}_s \bar{\mathbf{B}} + p_{xj} \bar{\bar{\mathbf{F}}}_s \frac{\mathrm{d}\mathbf{V}}{\mathrm{d}p_{xj}} \tag{26}$$

where $\bar{\mathbf{B}} = \begin{bmatrix} \mathbf{b}^T(x_1) & \mathbf{b}^T(x_2) & \ldots & \mathbf{b}^T(x_n) \end{bmatrix}^T$ lists the equilibrium matrices of all monitored cross-sections. Finally, the derivative of $\mathbf{V}$ with respect to p_{xj} (Eq. (16)) becomes:

$$\frac{\mathrm{d}\mathbf{V}}{\mathrm{d}p_{xj}} = \mathbf{H}_\chi \bar{\mathbf{F}}_s \bar{\mathbf{B}} + p_{xj} \mathbf{H}_\chi \bar{\bar{\mathbf{F}}}_s \frac{\mathrm{d}\mathbf{V}}{\mathrm{d}p_{xj}} \tag{27}$$

or, collecting the terms and introducing a $n \times n$ identity matrix $\mathbf{I}_n$:

$$\left(\mathbf{I}_n - p_{xj} \mathbf{H}_\chi \bar{\bar{\mathbf{F}}}_s\right) \frac{\mathrm{d}\mathbf{V}}{\mathrm{d}p_{xj}} = \mathbf{H}_\chi \bar{\mathbf{F}}_s \bar{\mathbf{B}} \tag{28}$$

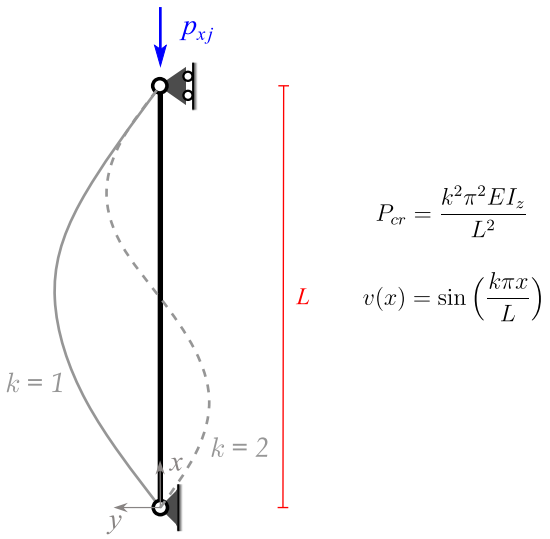

Fig. 4. Analytical solution for the critical buckling modes of a prismatic column.

Critical buckling is obtained when the matrix in parentheses of Eq. (28) is singular or, equivalently, when p_{xj} satisfies the eigenvalue problem $\left(\mathbf{I}_n - p_{xj} \mathbf{H}_\chi \bar{\bar{\mathbf{F}}}_s\right) \mathbf{V} = \mathbf{0}$, for a non-zero vector $\mathbf{V}$, that is, by changing the sign of p_{xj} so that compressive axial force is positive, for the eigenpairs $\left\{\lambda = \frac{1}{p_{xj}}; \mathbf{V}\right\}$ that solve the following eigenproblem:

$$\left(-\mathbf{H}_\chi \bar{\bar{\mathbf{F}}}_s\right) \mathbf{V} = \lambda \mathbf{V} \tag{29}$$

i.e., the eigenvalues and eigenvectors of matrix $\mathbf{A} = -\mathbf{H}_\chi \bar{\bar{\mathbf{F}}}_s$.

To be noted is that, assumed that the two end cross-sections of the element are included in the set, this approach permits to compute the first $n - 2$ buckling modes.

Moreover, it is worth to remark that the procedure presented hereafter is valid for columns with simply-supported end restraints (Fig. 1). Extension to different boundary conditions is possible by modification of matrix $\mathbf{H}_\chi$, governing Eq. (4). This would enable the analysis of a wider range of real-world samples, such as aging cantilevered bridge piers. However, the discussion of this extension is beyond the scope of this work and is left for future studies.

4. Numerical applications

To address the performance of the proposed procedure based on the FDDI and show that this does not suffer from numerical issues, two of the numerical tests conducted in [11] are considered in the following: a simple prismatic column and a column with a weakened cross-section.

For all numerical analyses, the monitored cross-sections are assumed as equally spaced along the column length, and the two column end points are included (as in the Trapezoidal quadrature rule). Moreover, the FDDI technique always adopts a 5-point FD scheme (FDDI5). For the CBDI technique, the inverse of the Vandermonde matrix $\mathbf{G}$ (Eqs. (7) and (8)) is computed through the Moore–Penrose pseudoinverse [21] to show that, regardless of the numerical improvement provided by the Moore–Penrose pseudoinverse, the technique is still unstable for large numbers of quadrature cross-sections. Computations are performed is Matlab®, version 2023b.

4.1. Prismatic column

A linear elastic column with length L and uniform flexural inertia EI_z is considered. Fig. 4 shows the reference configuration and the

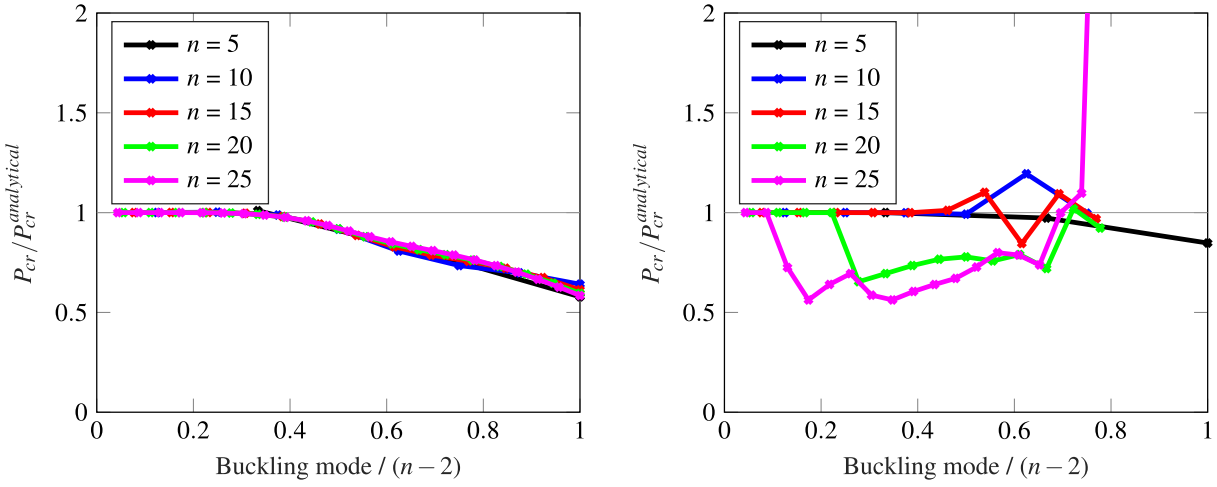

(a) FDDI (b) CBDI

Fig. 5. Normalized buckling loads of the prismatic column for an increasing number of monitored cross-sections. (For interpretation of the references to color in this figure legend, the reader is referred to the web version of this article.)

first two buckling mode shapes resulting from the standard analytical solution, reported in the same picture, being k the mode number.

The numerical solution obtained with the proposed approach uses a $n \times n$ diagonal matrix $\bar{\bar{\mathbf{F}}}_s = \text{diag}\left\{\frac{1}{EI_z}, \frac{1}{EI_z}, \dots, \frac{1}{EI_z}\right\}$ and provides the first $n-2$ buckling modes as eigenvalues and eigenvectors of matrix $\mathbf{A} = -\mathbf{H}_\chi \bar{\bar{\mathbf{F}}}_s$.

The precision of this solution is investigated in Fig. 5 This shows the buckling loads for (a) the FDDI and (b) the CBDI technique, normalized with respect to the corresponding analytical values, for an increasing number n of monitored cross-sections. The approach using the FDDI technique is always stable and converges to the exact solution (normalized value equal to 1) as n grows. In fact, the curves in Fig. 5a show that, for a given n, the method always provides accurate values of the first 40% of the $n-2$ available buckling modes; while, the error on the remaining modes is lower than 50%. As a result, as n increases, an increasing number of modes is accurately obtained.

The CBDI does not show the same trend, as observed in [11]. Although the solution is accurate for low values of n, and even more precise of the FDDI, it starts to diverge from the analytical one as n increases, due to the numerical errors in matrix $\mathbf{H}_\chi$. The work in [20] demonstrates that this is due to the ill-conditioning of the Vandermonde matrix $\mathbf{G}$, whose inverse is required in Eq. (7). Although the Moore–Penrose pseudoinverse is adopted to compute $\mathbf{G}^{-1}$, in the buckling analysis, this ill-conditioning leads to an eigensolution where the higher buckling loads appear as complex conjugate pairs. The values of the normalized stability variable $\frac{P_{cr}L^2}{EI_z}$ are reported in Table 1. Similar observations hold for the buckling mode shapes plotted in Fig. 6 for (a) $n = 5$, (b) $n = 10$ and (c) $n = 20$.

Notably, to perform the plot in Fig. 5b, the complex magnitude (complex norm) of the complex buckling loads is considered as critical load value.

4.2. Weakened column

Wang et al. [5] derived an analytical solution for the first buckling load of a prismatic Euler–Bernoulli column under uniform axial force, assuming that the cross-section at a certain location a along the height L is weaker than the remainder of the column. This solution is derived by modeling the column as two segments hinged at a and adding a discrete rotational spring with stiffness $\gamma = \frac{k\,EI_z}{L}$ (Fig. 7), being $k \le 1$ a stiffness scaling coefficient.

Table 1
Values of the stability variable $\frac{P_{cr}L^2}{EI_z}$ obtained for the prismatic column with the CBDI technique.

Buckling mode	Monitored cross-sections			
	5	10	15	20
1	9.87	9.87	9.87	9.87
2	38.40	39.48	39.48	39.48
3	75.29	88.76	88.83	88.83
4		156.68	157.91	157.91
5		$333.96 \pm 117.98\,i$	246.63	161.31
6		$293.29 \pm 28.83\,i$	359.35	246.74
7			$755.52 \pm 586.45\,i$	355.36
8			$744.85 \pm 458.80\,i$	484.11
9			$530.33 \pm 49.78\,i$	$1252.20 \pm 1271.90\,i$
10			533.93	$1287.10 \pm 1111.40\,i$
11				622.09
12				748.17
13				$956.85 \pm 362.77\,i$
14				$913.15 \pm 236.34\,i$

In [11], the same column is analyzed with the proposed numerical procedure by averaging the effects of the discrete spring. Specifically, the first buckling load of the column is obtained as the first eigenvalue of matrix $\mathbf{A} = -\mathbf{H}_\chi \bar{\bar{\mathbf{F}}}_s$, where $\bar{\bar{\mathbf{F}}}_s$ is the $n \times n$ flexibility matrix defined as:

$$\bar{\bar{\mathbf{F}}}_s = \text{diag}\left\{\frac{1}{EI_z}, \dots, \frac{1}{EI_z}, \frac{1}{\alpha\,EI_z}, \frac{1}{EI_z}, \dots, \frac{1}{EI_z}\right\} \tag{30}$$

i.e., where the flexibility of the cross-section located at a is increased through factor α. The value of α is obtained considering that the flexibility $f_{spring} = \frac{1}{\gamma}$ of the discrete rotational spring is in series with the flexibility $f_{column} = \frac{L_a}{EI_z}$ of the column over the length L_a, associated to the corresponding monitored cross-section. For equally-spaced cross-sections that include the two ends of the column, it results $L_a = \frac{L}{n-1}$, as in the trapezoidal quadrature rule. Hence, the equivalent column flexibility $f^{eq}_{column} = \frac{L_a}{\alpha\,EI_z}$ that accounts for the spring is equal to:

$$f^{eq}_{column} = \frac{L_a}{\alpha EI_z} = f_{spring} + f_{column} = \frac{L}{k\,EI_z} + \frac{L_a}{EI_z} \tag{31}$$

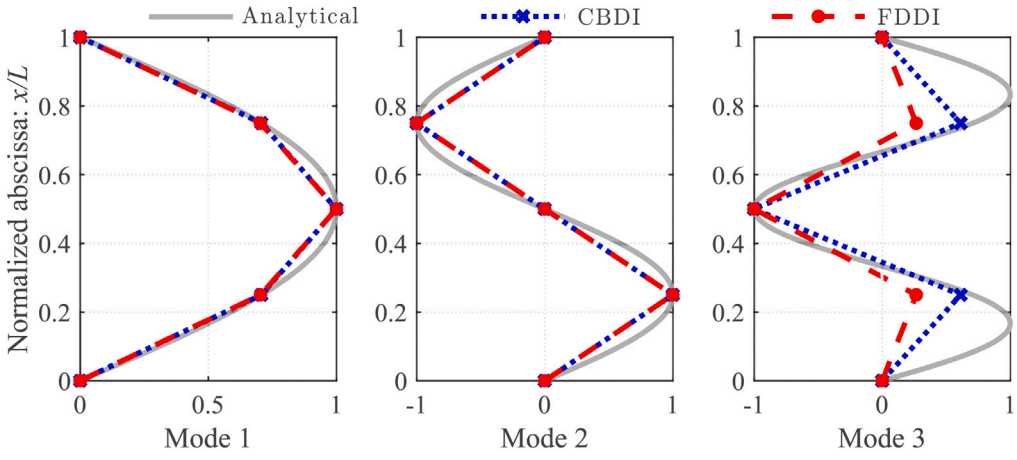

(a) $n = 5$

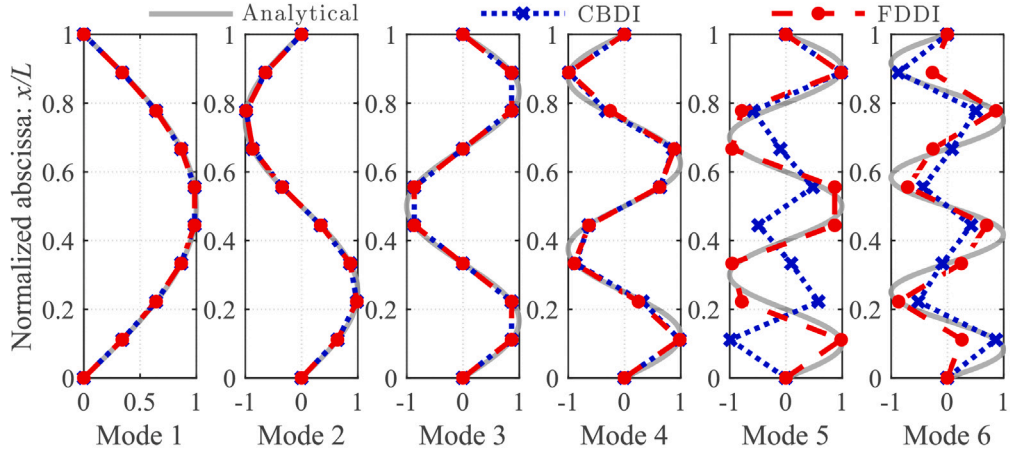

(b) $n = 10$

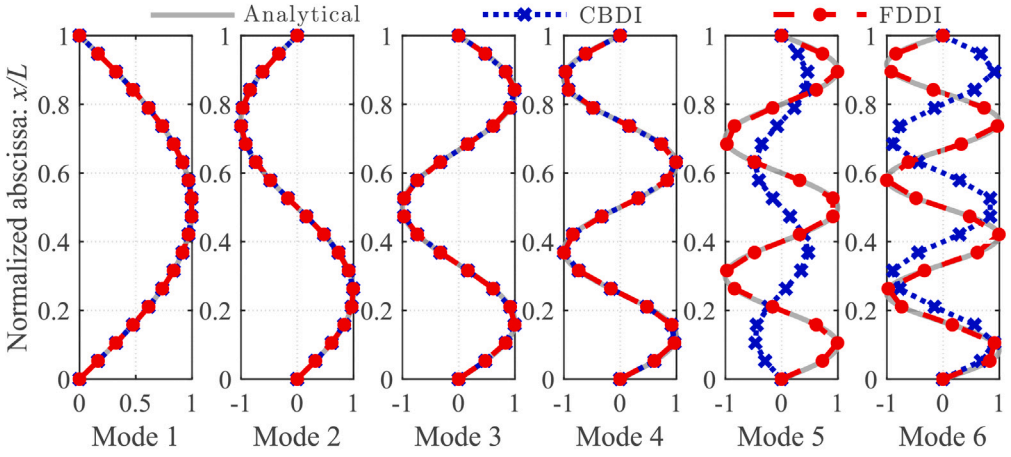

(c) $n = 20$

Fig. 6. Buckling mode shapes of the prismatic column obtained for an increasing number of monitored cross-sections.

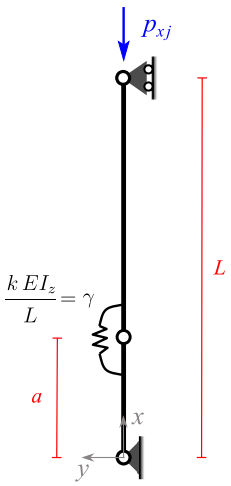

Fig. 7. Simply-supported column with a discrete rotational spring.

Hence, solving Eq. (31) for α gives:

$$\alpha = \frac{k}{k+n-1} \tag{32}$$

Fig. 8 compares the numerical results achieved with the CBDI (dotted blue curves with crosses) and FDDI (dashed red curves with dots) techniques, for different values of k, adopting (a) 6, (b) 9, (c) 12, (d) 15 and (e) 51 monitored cross-sections for the entire column. The analytical solution in [5] (solid dark gray curves) is also plotted for reference.

Moreover, for the case $n = 51$ (Fig. 8e), a second reference solution is reported (black crosses). This is obtained by performing buckling analysis in Abaqus finite element software. For this analysis, the column is modeled with the B21 2-node beam elastic elements, adopting a uniform mesh with element size of $L/100$. To avoid shear deformation influence, the actual computation is performed considering $L = 1\,\text{m}$ and a square cross-section of size 0.01 m.

As in the prismatic column test, the CBDI offers adequately reliable results only for low values of n. When the number of monitored cross-sections is increased to enhance the solution, the technique diverges due to numerical issues, despite the use of the Moore–Penrose pseudoinverse. In contrast, the FDDI technique consistently converges to the analytical results, even for very high values of n, as illustrated in Fig. 8e for $n = 51$.

Table 2 and Fig. 9 report the first seven buckling loads and mode shapes, respectively, derived using the FDDI technique for $n = 51$ (solid red curves), and considering two weakening levels ($k = 5$ and 0.5) and two positions of the weakened cross-section ($a/L = 0.2$ and 0.5). These practically coincide with the Abaqus solution, reported in the same plots as dashed black curves. As expected, when k increases, the stiffness of the column becomes more involved in the buckling modes than that of the discrete spring and the buckling load increases. This also increases when the weakened cross-section is placed far away from the mid-height.

It is interesting to note that, when the weakened cross-section is at mid-height, i.e. $a/L = 0.5$ (Figs. 9b and c), modes 2, 4, and 6 do not depend on the weakening parameter k, as these modes do not trigger the deformation of the mid-height cross-section and, thus, are the same as for a intact column.

5. Conclusions

This work explores the use of the Finite Difference Displacement Integration (FDDI) [20] for the numerical procedure proposed by Scott and Denavit [11] to compute the buckling modes of columns with arbitrarily variable stiffness along the height. The procedure is based on the eigenvalue analysis of matrix $\mathbf{H}_\chi$, relating the transverse displacements of the column to the bending curvatures, multiplied by the cross-section flexibility matrix $\bar{\bar{\mathbf{F}}}_s$.

In the original proposal [11], matrix $\mathbf{H}_\chi$ is the influence matrix of the Curvature Based Displacement Interpolation (CBDI) [12,13], which becomes ill-conditioned when many quadrature cross-sections are placed along the element. In the present work, maintaining the exact same architecture of the procedure, the definition of matrix $\mathbf{H}_\chi$ is replaced with that resulting from the FDDI technique, expressing, in a similar fashion, the FD approximation of the transverse displacement second order derivative.

The numerical tests reveal that using the FDDI effectively permits to avoid the numerical issues associated with the CBDI. The use of several cross-sections along the column height is crucial for capturing the precise values of the critical buckling loads, especially when higher modes are of interest. In these cases, the CBDI technique fails to describe the column buckling behavior, diverging from the correct solution. In contrast, the FDDI technique is always stable and converges to the exact results. For low values of n, where the CBDI remains reliable, the FDDI achieves a similar level of accuracy without increasing the computational cost.

Hence, with the introduction of the FDDI technique, the proposed numerical procedure is an accurate simple method to numerically evaluate the buckling response of columns with variable cross-section geometry, weakened at interior locations or undergoing nonlinear yielding and damage. In situations where the flexural stiffness of a column varies along its height, this computation necessitates the employment of complex numerical approaches, such as finite element analysis. Consequently, advanced finite element software capable of performing buckling analysis is required. In contrast, the proposed method can be efficiently implemented in various programming languages (e.g., Matlab® or Python) with minimal coding effort, thereby providing a fast, yet reliable, solution.

It is important to note that the methodology described in this study refers to simply-supported columns, under the assumption of Euler–Bernoulli beam theory. Nevertheless, by exploiting the FD approach, this methodology can be seamlessly extended to accommodate various boundary conditions, thereby permitting the analysis of a wide range of real-world specimens, including deteriorating cantilevered bridge piers. Furthermore, the effects of shear deformations could be incorporated.

Table 2
Values of the stability variable $\frac{P_{cr}L^2}{EI_z}$ obtained for the weakened column with the FDDI technique for $n = 51$.

Buckling mode	Weakened cross-section parameters			
	$k = 5$ $a/L = 0.2$	$k = 5$ $a/L = 0.5$	$k = 0.5$ $a/L = 0.2$	$k = 0.5$ $a/L = 0.5$
1	8.45	6.91	2.65	1.71
2	28.23	39.48	16.87	39.48
3	72.09	65.34	63.15	43.83
4	147.15	157.91	140.43	157.91
5	246.73	192.28	246.73	163.69
6	300.99	355.28	257.35	355.28
7	402.65	394.69	388.20	363.25

Declaration of competing interest

The authors declare that they have no known competing financial interests or personal relationships that could have appeared to influence the work reported in this paper.

Acknowledgments

P.D.R. acknowledges the research project PRIN-2022 – B53D23006 300006.

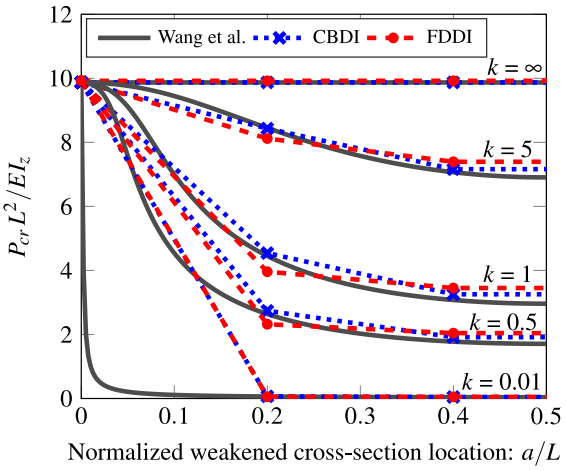

(a) $n = 6$

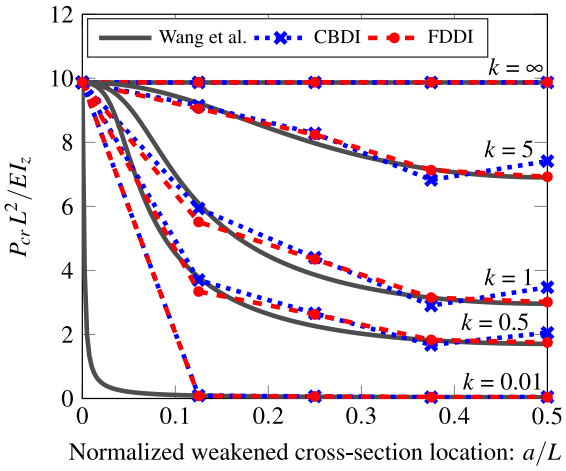

(b) $n = 9$

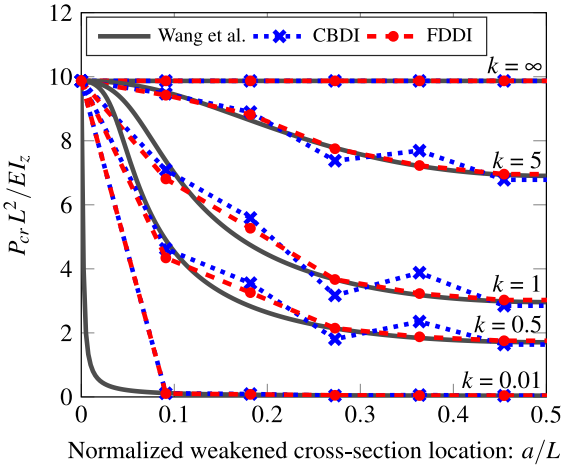

(c) $n = 12$

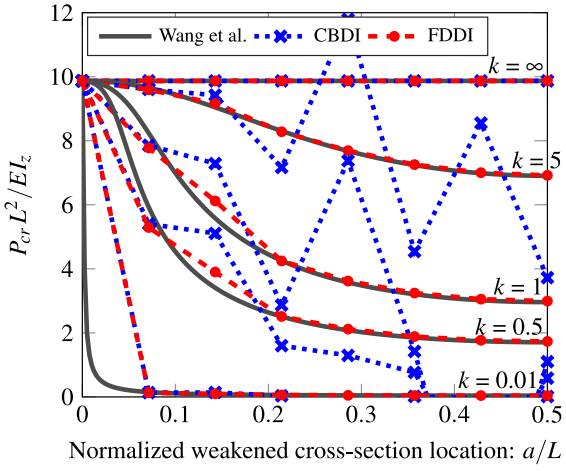

(d) $n = 15$

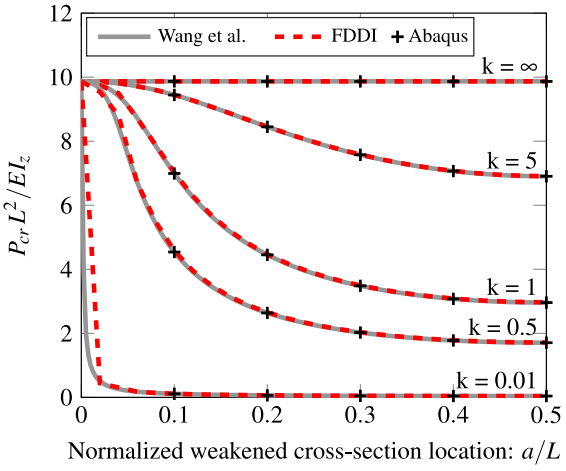

(e) $n = 51$

Fig. 8. Values of the stability variable $\frac{P_{cr}L^2}{EI_z}$ obtained for the first buckling mode of the weakened column.

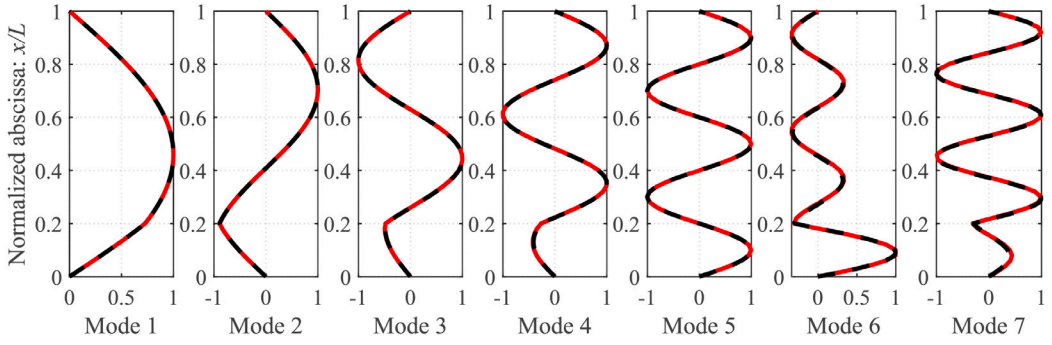

(a) $k = 5$ and $a/L = 0.2$

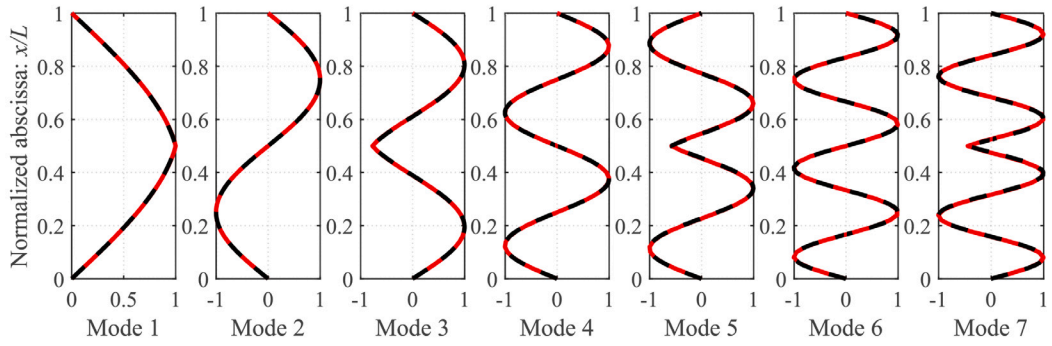

(b) $k = 5$ and $a/L = 0.5$

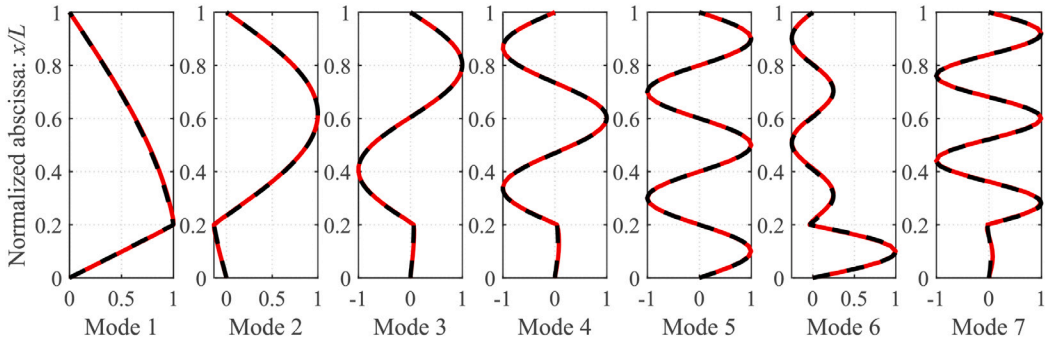

(c) $k = 0.5$ and $a/L = 0.2$

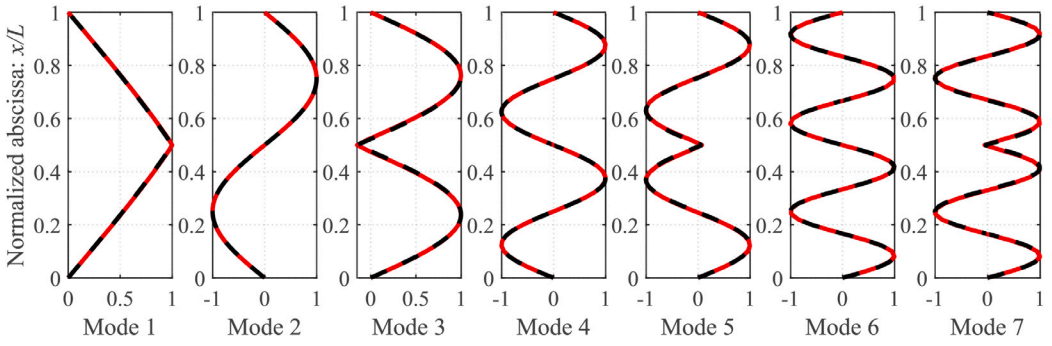

(d) $k = 0.5$ and $a/L = 0.5$

Fig. 9. Buckling mode shapes obtained for the weakened column: red solid curves for the FDDI technique with $n = 51$ and black dashed curves for the Abaqus solution. (For interpretation of the references to color in this figure legend, the reader is referred to the web version of this article.)

Data availability

Data will be made available on request.

References

[1] Q.S. Li, Classes of exact solutions for buckling of multi-step non-uniform columns with an arbitrary number of cracks subjected to concentrated and distributed axial loads, Internat. J. Engrg. Sci. 41 (6) (2003) 569–586.

[2] J.A. Loya, G. Vadillo, J. Fernandez-Saez, First-order solutions for the buckling loads of Euler-Bernoulli weakened columns, J. Eng. Mech. 136 (5) (2010) 674–679.

[3] Y. Huang, X.F. Li, Buckling analysis of nonuniform and axially graded columns with varying flexural rigidity, J. Eng. Mech. 137 (1) (2011) 73–81.

[4] G. Vadillo, J.A. Loya, J. Fernandez-Saez, First order solutions for the buckling loads of weakened Timoshenko columns, Comput. Math. Appl. 64 (8) (2012) 2395–2407.

[5] C.Y. Wang, C.M. Wang, T.M. Aung, Buckling of a weakened column, J. Eng. Mech. 130 (11) (2004) 1373–1376.

[6] N. Challamel, C. Lanos, C. Casandjian, Localization in the buckling or in the vibration of a two-span weakened column, Eng. Struct. 28 (5) (2006) 776–782.

[7] L.G. Arboleda-Monsalve, D.G. Zapata-Medina, J.D. Aristizabal-Ochoa, Stability and natural frequencies of a weakened Timoshenko beam-column with generalized end conditions under constant axial load, J. Sound Vib. 307 (1) (2007) 89–112.

[8] D.G. Zapata-Medina, L.G. Arboleda-Monsalve, J.D. Aristizabal-Ochoa, Static stability formulas of a weakened Timoshenko column: Effects of shear deformations, J. Eng. Mech. 136 (12) (2010) 1528–1536.

[9] M.J. Iremonger, Finite difference buckling analysis of non-uniform columns, Comput. Struct. 12 (5) (1980) 741–748.

[10] M. Mahmoudabadi, S.M.R. Hasani, R. Akbari, The study of elastic buckling load of uniform & non-uniform columns under non-uniform axial loading using finite element method, J. Struct. Constr. Eng. 8 (2) (2021) 141–158.

[11] M. Scott, M. Denavit, Generalized computation of buckling loads via curvature-based displacement interpolation, J. Struct. Eng. 149 (2) (2023) 04022231.

[12] A. Neuenhofer, F. Filippou, Geometrically nonlinear flexibility-based frame finite element, J. Struct. Eng. 124 (6) (1998) 704–711.

[13] R. De Souza, Force-Based Finite Element for Large Displacement Inelastic Analysis of Frames (Ph.D. thesis), University of California, Berkeley, CA, United States, 2000.

[14] V. Jafari, S. Vahdani, M. Rahimian, Derivation of the consistent flexibility matrix for geometrically nonlinear Timoshenko frame finite element, Finite Elem. Anal. Des. 46 (12) (2010) 1077–1085.

[15] M. Rezaiee-Pajand, N. Gharaei-Moghaddam, Analysis of 3D Timoshenko frames having geometrical and material nonlinearities, Int. J. Mech. Sci. 94–95 (2015) 140–155.

[16] M.H. Scott, V. Jafari Azad, Response sensitivity of material and geometric nonlinear force-based Timoshenko frame elements, Internat. J. Numer. Methods Engrg. 111 (5) (2017) 474–492.

[17] D. Feng, X. Chen, F. McKenna, E. Taciroglu, Consistent nonlocal integral and gradient formulations for force-based Timoshenko elements with material and geometric nonlinearities, J. Struct. Eng. 149 (4) (2023) 04023018.

[18] P. Di Re, D. Addessi, C. Gatta, L. Parente, E. Sacco, Corotational force-based beam finite element with rigid joint offsets for 3D framed structures, Comput. Methods Appl. Mech. Engrg. 419 (2024) 116656.

[19] M. Sivaselvan, A. Reinhorn, Collapse analysis: large inelastic deformations analysis of planar frames, J. Struct. Eng. 128 (12) (2002) 1575–1583.

[20] P. Di Re, D.M. Benaim Sanchez, Finite difference technique for the evaluation of the transverse displacements in force-based beam finite elements, Comput. Methods Appl. Mech. Engrg. 428 (2024) 117067.

[21] R. MacAusland, The Moore-Penrose Inverse and Least Squares, Advanced Topics in Linear Algebra, University of Puget Sound. Math 420, 2014.

[22] G. Strang, Linear Algebra and Its Applications, Cengage India, 2012.

[23] K. Bathe, Finite Element Procedures, Prentice Hall, Pearson Education Inc., 2006.

[24] R.J. LeVeque, Finite Difference Methods for Ordinary and Partial Differential Equations: Steady-State and Time-Dependent Problems, Society for Industrial and Applied Mathematics, 2007.

[25] H. Langtangen, S. Linge, Finite Difference Computing With PDEs: A Modern Software Approach, Springer Nature, 2017.

[26] B. Cheong Khoo, J. White, J. Peraire, A. Patera, Lecture Notes of the Course "Numerical Methods for Partial Differential Equations (SMA 5212)", Online resource. URL: https://ocw.mit.edu/courses/16-920j-numerical-methods-for-partial-differential-equations-sma-5212-spring-2003/pages/lecture-notes/. (Accessed 23 July 2023).

[27] B. Fornberg, Generation of finite difference formulas on arbitrarily spaced grids, Math. Comp. 51 (184) (1988) 699–706.